International Journal of Fracture **117:** 101–112, 2002.
© 2002 *Kluwer Academic Publishers. Printed in the Netherlands.*

Impact fracture of a ferritic steel in the lower shelf regime

D. RITTEL[1], B. TANGUY[2], A. PINEAU[2] and T. THOMAS[3]
[1]*Faculty of Mechanical Engineering, Technion, 32000 Haifa, Israel*
[2]*Ecole des Mines de Paris, Centre des Matériaux P.M. Fourt, BP 87, 91003 Evry Cedex, France*
[3]*Centre Technique de l'Armement, 16 bis Av. Prieur de la Côte d'Or, 94114 Arcueil Cedex, France*

Received 22 June 2001; accepted 3 July 2002

Abstract. This paper reports the results of a systematic investigation on the fracture of Charpy-V notch A508 steel specimens, tested in the lower shelf regime. The fracture energy has been determined for quasi-static, standard Charpy and one-point-bend impact. The results show a general trend for the fracture energy to increase with the loading rate, at the lower temperature (~ -160 °C). At this temperature, the roughness of the fracture surface increases markedly with the loading rate. The fractographic analysis shows the presence of 3–4 cleavage initiation sites situated at 100–800 μm from the crack front, irrespective of the loading rate. Numerous cleavage microcracks are observed underneath the main fracture plane. The statistical analysis shows that the length distribution of the microcracks is adequately described by Weibull statistics. It is also found that the number of microcracks increases with the loading rate. It is suggested that the larger number of microcracks is responsible for the observed increased roughness and energy dissipation.

Key words: Charpy test, one-point-bend impact, dynamic fracture, fracture energy, ferritic steel, roughness, Weibull.

1. Introduction

Impact fracture response of materials is generally addressed at two distinct levels: the first deals with *dynamic fracture mechanics* concepts to characterize the dynamic fracture toughness, at the initiation, propagation and arrest stages (see e.g., Rosakis and Ravichandran, 2000). Another aspect relates to the *impact properties*, i.e. the characterization of a global fracture energy as in the case of the popular Charpy test (Charpy, 1901). Charpy tests are carried out according to a well-established procedure, which specifies the specimen geometry and loading apparatus. The impact velocity of the standard Charpy test pendulum is about 5 m/s. However, experiments have been carried out using a modified split Hopkinson pressure bar concept to apply higher impact velocities to a three point bend specimen (Ruiz and Mines, 1985). In dynamic experiments of either kind, two important experimental issues arise in these tests: the first concerns the nature of the boundary conditions related to the contact between the specimen and the supports (Böhme and Kalthoff, 1982), and the second is the determination of the onset of fracture from the acquired data (loads, displacements), as noted by several authors (Böhme, 1990; Aoki and Kimura, 1993; Maigre and Rittel, 1996; Radakovic et al., 1999). Recently, Rittel et al. (2002) performed one-point bend impact experiments on tempered bainitic A508 steel Charpy specimens. The tests were carried out in the range of temperatures corresponding to the lower shelf regime, so that the specimens fully fractured by cleavage. The main results of this study were that meaningful high velocity impact tests (typically 25 m/s) could be carried out for sufficiently brittle materials. The fracture time was assessed by means of fracture gages and high-speed photography, and an excellent correspondence between these

Table 1. Nominal specimen composition in w/o (Fe bal.).

C	S	P	Si	Mn	Ni	Cr	Mo	Cu	Co	V
0.16	0.004	0.008	0.22	1.33	0.76	0.22	0.51	0.07	0.0017	<0.01

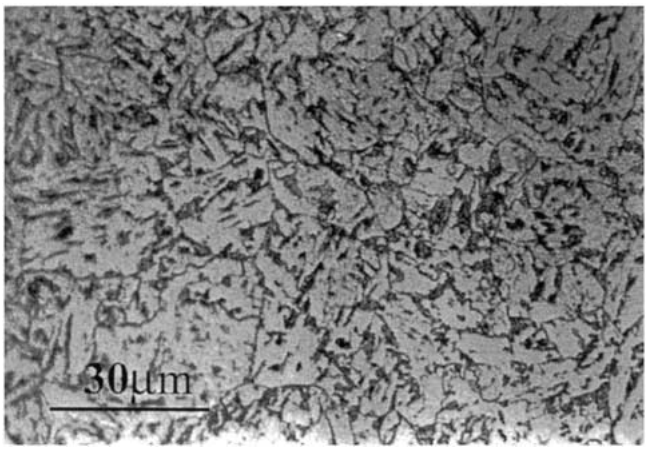

Figure 1. Typical tempered bainitic microstructure of the investigated steel. Etchant: Nital 3%.

two indications was noted. Fracture energy was assessed by integrating the product of the applied load by the displacement over a time period ranging from the onset of the impact until fracture time.

Our previous results addressed essentially *experimental aspects* of the problem. The present paper gives additional new results pertaining to the *nature of the failure processes* operating at various loading velocities. Three specific loading configurations were investigated, two dynamic (conventional Charpy and one-point bend impact) and the other quasi-static. All the experiments were carried out on conventional Charpy specimens. The following issues are addressed: firstly a comparison is made of the methods used to assess the fracture energies in the two dynamic tests. The fracture energies are then reported for each testing configuration. Next, the failure mechanisms, which characterize each test, are reported and compared both at the macroscopic and microscopic scale by means of a detailed microstructural and fractographic analysis. The results are then discussed, followed by a concluding section.

2. Experimental

2.1. Material

The material selected for this study is a French steel (16MND5) of composition given in Table 1, which corresponds to A508 steel. This steel is used in the nuclear industry for pressure water vessel applications. The material was heat treated to a hardness HV (20g)=200, with room temperature yield strength of $\sigma_y = 500$ MPa, tensile strength $\sigma_{\text{uts}} = 620$ MPa, and tensile elongation el $= 10.6\%$.

A typical microstructure is shown in Figure 1, which clearly illustrates the tempered bainitic microstructure of the material.

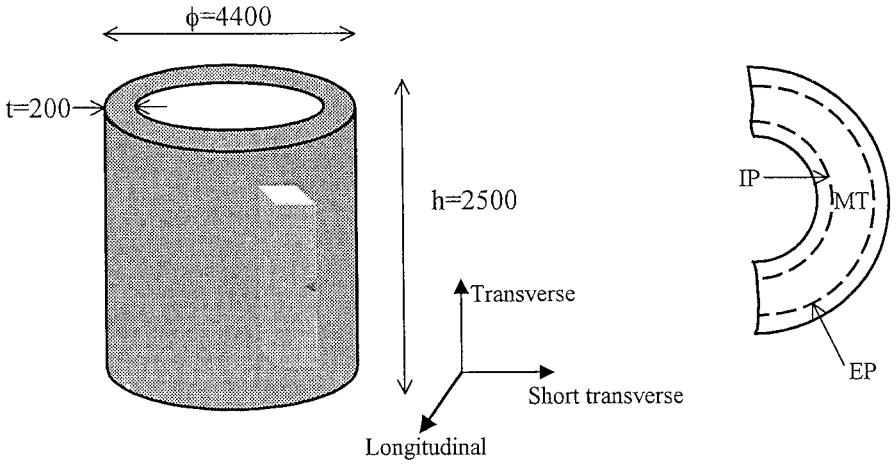

Figure 2. Schematic representation of the specimens' orientations in the pressure vessel.

2.2. SPECIMENS

Standard Charpy V (45degrees) notch specimens were machined and used throughout the tests. TL specimens were extracted form the cylindrical pressure vessel with the notch aligned with the L direction, as shown in Figure 2. All the specimens were machined from a layer located at 20–80% of the thickness, to minimize skin effects on the material homogeneity. The position of each specimen is indicated in Table 2, where IP ($\sim$ 50 mm distant from the internal vessel wall thickness), EP ($\sim$ 50 mm distant from the external wall thickness) and MT (mid thickness) designate the internal position, external position and mid–thickness, respectively.

2.3. TESTING AND DATA PROCESSING

2.3.1. *Quasi-static Charpy testing*

Three-point bend experiments were carried out at a prescribed crosshead velocity of 0.5 mm/s using a 250 kN Instron machine with a special set-up which was machined to have the same contact conditions (tup and anvils) as those of a conventional Charpy impact machine. The fracture energy was determined by integrating the area under the load-displacement curve, in which the compliance of the loading train had been taken into account.

2.3.2. *Conventional Charpy testing*

Conventional Charpy testing was carried out on an instrumented Amsler RHP300 machine with an energy capacity of 300 Joules. The average energy loss due to pendulum friction was determined prior to testing and found to be about 1 Joule. The reported impact energy values were conventionally determined from the gage reading minus the previously mentioned losses. The fracture energy was also determined in a separate procedure from the instrumented recordings of the load and displacement. For the sake of brevity, this procedure will not be detailed here. It will only be mentioned that a good agreement was obtained between gage reading corrected from pendulum friction and instrumented energy results. The specimen temperature was monitored and controlled by cementing a thermocouple to the specimen.

2.3.3. *High velocity Charpy testing*

High velocity Charpy testing procedure has been described in detail in Rittel et al. (2001) and will only be briefly outlined here.

The specimen temperature was determined from a previously established calibration curve showing the specimen temperature as a function of time, following specimen extraction from a liquid nitrogen bath. To establish this curve, two thermocouples had been cemented, one on the surface and the other at mid-thickness of the specimen, as in Rittel (1998). Temperature records showed almost no difference between surface and core temperatures.

In the impact test, the specimen is brought in contact with an instrumented bar and allowed to reach the desired temperature. Stress wave loading of the specimen is controlled by firing a striker on the other end of the bar. The specimen is not supported and fractures by its own inertia. The incident (ε_{in}) and reflected (ε_{ref}) gage signals are measured on the bar. Fracture time (t_f) is determined by means of single wire fracture gages. The fracture energy (E_f) is given by the following expression:

$$E_f = Ac_0E\int_0^{t_f}[\varepsilon(\alpha)_{\text{in}}^2 - \varepsilon(\alpha)_{\text{ref}}^2]\text{d}\alpha, \tag{1}$$

Where A and E are the bar cross-section (8×10 mm^2) and Young's modulus ($E = 210$ GPa) respectively, and c_0 is the longitudinal wave velocity (4700 m/s).

2.3.4. *Recrystallization technique*

It is well known that metallic materials tend to recrystallize when subjected to a heat treatment. The extent of the recrystallization is related to the prior plastic deformation. The recrystallization technique to estimate the notch plastic strains has already been used in A508 steel (Lautridou and Pineau, 1981; Tanguy et al., 2000). In the present study, selected fractured specimens were subjected to a recrystallization heat treatment in vacuum at 695 °C for 4 h. The fracture surface was then nickel plated and sectioned at mid-thickness, perpendicular to the fracture plane. The specimen was prepared by standard metallographic technique for microstructural characterization. The average notch strain was estimated from the recrystallized grain size, on the basis or a previous calibration relating the average grain size to the plastic strain in the material of this study (Tanguy et al., 2000). Previous results showed that this technique is effective, in the sense that recrystallization is clearly discernable, when the local effective plastic strain exceeds ~ 0.20.

3. Results

3.1. Fracture energy

The fracture energy and experimental conditions of each specimen tested in the lower shelf regime are given in Table 2. When comparing high velocity and conventional Charpy tests, it is noted that the fracture energy corresponding to high velocity testing is on the average 2 to 3 times greater than that measured in conventional tests carried out at a similar temperature. At a temperature of about -160 °C, the dynamic energies are also greater than the quasi-static. However, when the temperature is increased to about -120 °C, the quasi-static energy exceeds the Charpy energy. The observed variations do not appear to be related to the position of the specimens as shown by the comparison between I14 and H28 specimens both taken in the IP position.

Table 2. Experimental results and test temperatures. Paired values correspond to the use of 2 fracture gages, one on each side of the specimen. The applied velocity for dynamic tests is the nominal value at the onset of impact.

Specimen	Test	Temperature (°C)	Position	Velocity (m/s)	Fracture energy (J)
I14	Quasi-static	−160	IP	5e-6	2.79
I12	Quasi-static	−120	IP	5e-6	20.70
I37	Charpy	−166	MT	5	3.44
I34	Charpy	−120	MT	5	5.77
H28	1PB	−157	IP	20	8.90
H29	1PB	−148	IP	25	9.00
E14	1PB	−148	EP	22	10.33–11.03
H30	1PB	−136	IP	25	8.50
H31	1PB	−136	IP	25	11.24
E13	1PB	−136	EP	22	7.80-8.05
E15	1PB	−134	EP	22	7.60-9.30
H33	1PB	−124	IP	25	11.10

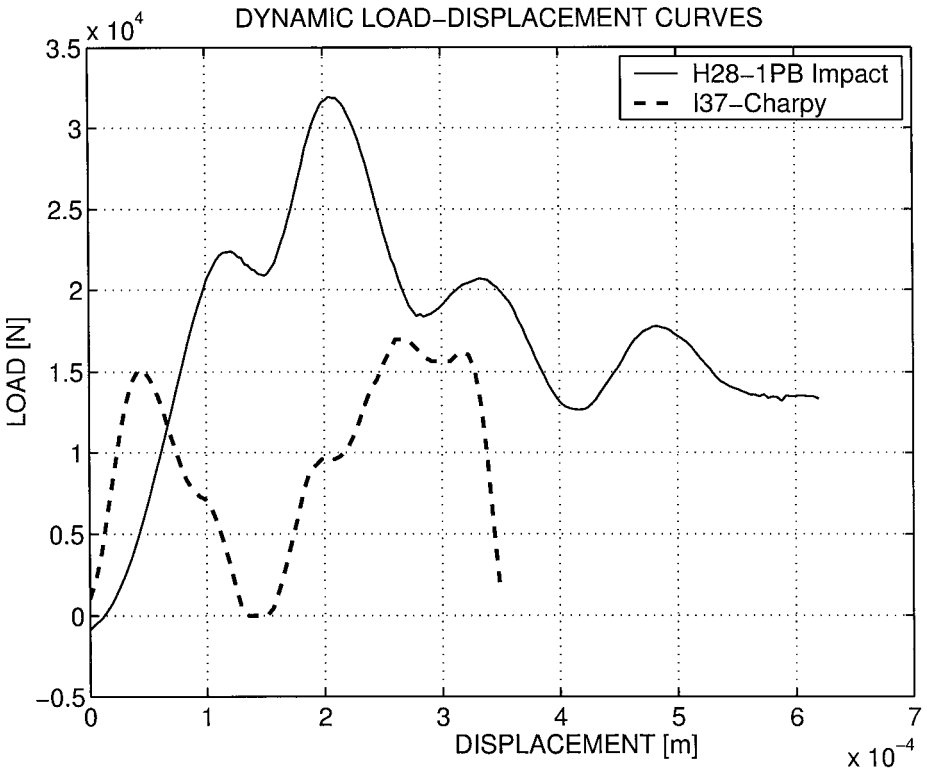

Figure 3. Typical dynamic load-displacement curves. Charpy and 1P- bend impact specimens. For the 1PB specimen, the curve has been truncated at the fracture time indicated by the fracture gage(s). For the Charpy specimen, the entire curve is displayed. Note the higher load and displacement levels experienced by the 1PB specimen.

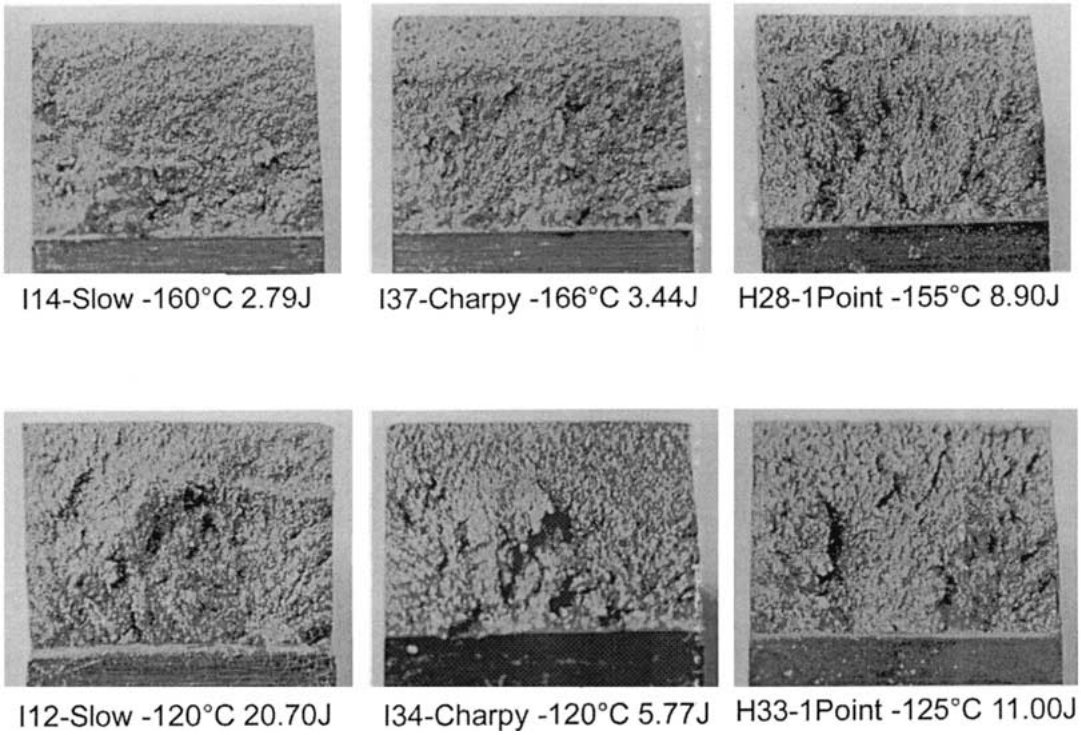

Figure 4. Macroscopic morphology of the fracture surfaces of Charpy specimens fractured at temperatures in the vicinity of −160 ∘C and −120 °C. The specimens have been tested quasi-statically, or by conventional Charpy or by 1PB impact. Note that at ∼ −160 °C, the fracture surface morphology is increasingly rougher with increasing loading rate. By contrast, at ∼ −120 °C, all fracture surfaces look equally rough.

Representative dynamic load-displacement curves are shown in Figure 3. For the high velocity tests, the curves have been truncated at the measured fracture load (displacement), which is the upper integration limit of the test (t_f in Equation (1)). For the conventional Charpy tests, the entire curve until presumed fracture is displayed. The overall load-displacement curves are similar as far as order of magnitudes are concerned. However, as expected, the high velocity tests are characterized by significantly higher loads and displacements until failure, when compared with the conventional tests. The particular shape of the Charpy curve indicates that the contact between the specimen and the tup is lost during a short period of time after about 0.15 ms.

3.2. Metallographic evaluation of the notch strains

The recrystallization experiments carried out on specimens fractured at ∼ −160 °C (I37, I14, H28) failed to show evidence of recrystallized grains, irrespective of the loading rate. This indicates that, in all cases, at low temperature the local notch-tip plastic strain was inferior to 0.20. It should be mentioned that at higher temperature (∼ −120 °C), previous studies on Charpy specimens showed that these notch strains were larger than 0.25 (Tanguy et al., 2000).

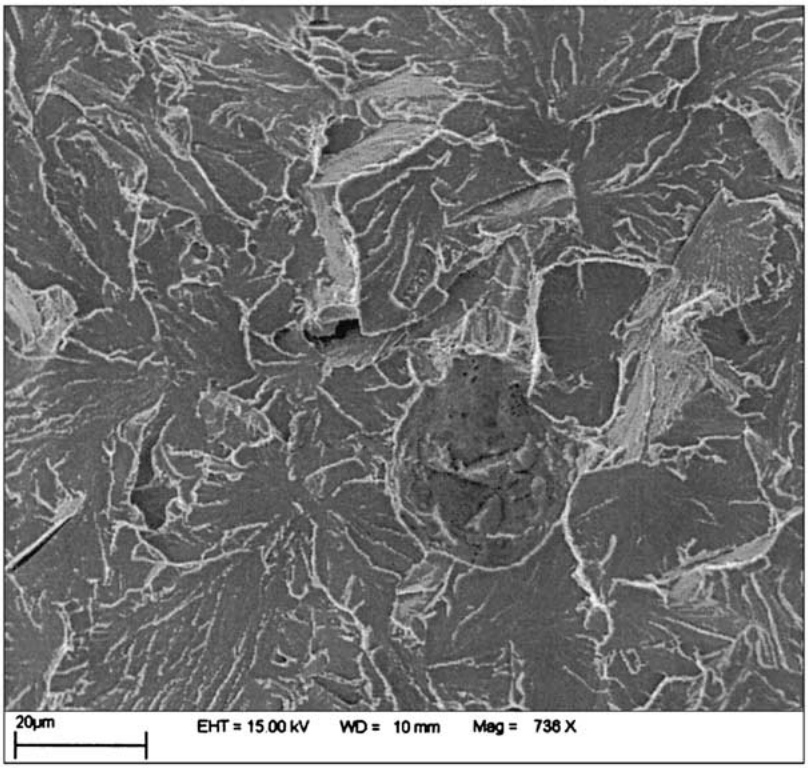

Figure 5. SEM fractograph of a typical cleavage origin in specimen H28 (probably a sulfide inclusion) at the center of the picture. No more than 3–4 such sources could be identified on the fracture surface of each specimen, irrespective of the loading velocity. A secondary cleavage microcrack is noticeable in the left corner.

3.3. Fractographic analysis

The morphology of the fracture surface of representative specimens is shown in Figure 4. Two test temperatures have been selected, in the vicinity of −160 °C and −120 °C. The specimens have been tested by conventional and high velocity impact tests. To allow for comparison, we have included specimens tested in three-point quasi-static bending at a prescribed crosshead speed of 0.5 mm/s. At the lowest test temperature, these macrographs reveal an increasing degree of roughness of the fracture surface with increasing test velocity. The specimen tested at high velocity is much rougher than that tested under quasi-static conditions. This trend becomes less obvious when the test temperature is increased to the vicinity of −120 °C.

Scanning electron microscopy (SEM) reveals cleavage as the main fracture mechanisms. Very narrow (typically 50 μm) discontinuous ligaments of ductile rupture precede the cleavage facets.

Additional information is gained from careful examination of the fracture surface at high magnification in the SEM, to identify the origin sites of cleavage fracture (carbides or inclusions), as shown in Figure 5. Careful examination of the specimens fractured at −160 °C revealed in every case the same typical 3 to 4 distinct origin sites for cleavage. The position of the initiating sites was found to be included between 100 and 800 microns from the notch tip. No systematic variation in the nature of initiating sites (carbides, inclusions) and in their position could be evidenced.

Table 3. Results of the statistical quantitative analysis of the cleavage microcracks observed underneath the main crack plane.

Specimen	Test	# Microcracks	Length (μm)	Std. dev. (μm)
I14	Quasi-static	91	310.0	173.5
H37	Charpy	126	366.9	226.7
H28	1PB	137	331.3	214.0

3.4. Secondary cracking below the main crack

Metallographic longitudinal sections were prepared perpendicular to the fracture plane, at specimen mid-thickness. Numerous cleavage cracks were observed underneath the main fracture path, as shown in Figure 6a. These secondary cracks were identified as connected with the main crack when they contained nickel plating. All the cracks, which were not connected with the main crack, were recorded for each specimen tested at -160 °C. The number of cracks and their average length is given in Table 3. It is noted that a greater number of microcracks was noted for the two dynamic specimens (I37 and H28) when compared with the quasi-static (I14). On the other hand their average length is independent of the loading rates. The length distribution of secondary cracks is shown in Figure 6b, using a Weibull plot.

4. Discussion

The low temperature toughness of A508 steel has been investigated at three loading rates, quasi-static, conventional Charpy and one-point bend impact. At the lowest temperature (about -160 °C), the impact toughness was noted to increase noticeably in the one-point bend test with respect to the other tests.

Two interesting issues arise from the present results and will therefore be discussed here. The first pertains to the *comparison between two dynamic testing techniques* and the significance of the measured results.

The second issue is that of the *physics of fracture*, when static or transient loads are applied. Specifically, what makes (if any) the difference between the two regimes?

4.1. A comparison between Charpy and one-point impact testing

Both methods measure the energy invested in the specimen until fracture. For the Charpy test, the energy is either measured directly from the dial or obtained through the integration of a load-displacement curve. The underlying assumption is that fracture is completed when the load has dropped to zero. It is well established that, at low impact energy, the analysis of the Charpy load-displacement curve is difficult, because it is strongly affected by inertial effects (see, e.g., Server, 1985). The one-point bend impact test provides a total energy to fracture in a similar way, with two important distinctions. First, the specimen is not supported, so that the boundary conditions are much simpler than those of a Charpy test. The second key point is that the onset of fracture is actually determined from the fracture gage reading without ambiguity. In a previous paper, Rittel et al. (2002) showed the excellent correspondence between fracture gage indications and high-speed photography, in this range of temperatures.

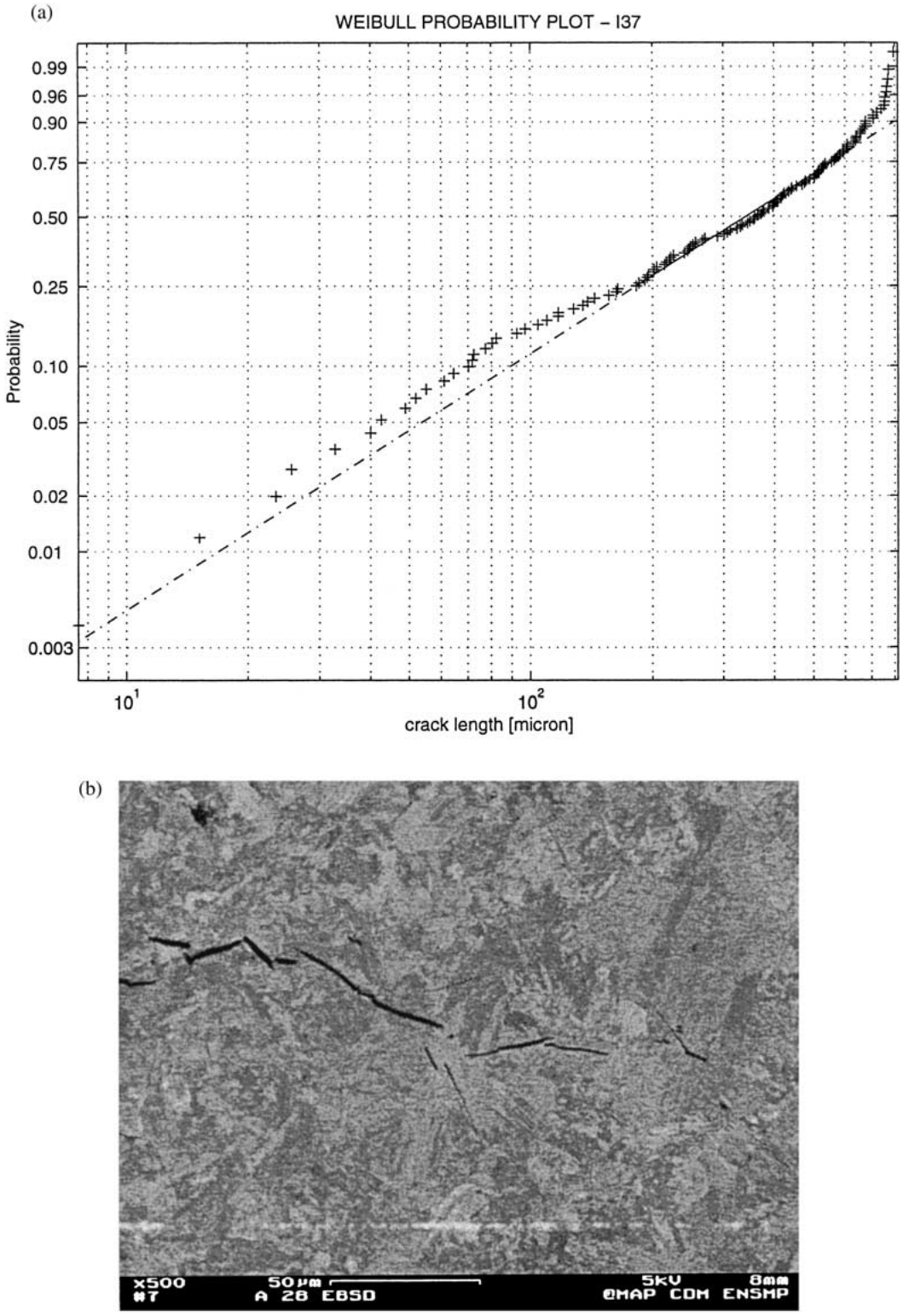

Figure 6. (a) Typical secondary cleavage microcracks lying underneath the main fracture plane. (b) Weibull plot of microcrack length distribution for specimen I37.

Table 4. Summary of the Weibull parameters of the microcrack distribution (specimens of Table 3).

Specimen	Test	b	95% CI limits	l_0 (μm)
I14	Quasi-static	1.75	1.47 – 2.03	349
I37	Charpy	1.55	1.30 – 1.80	407
H28	1PB	1.45	1.26 – 1.65	368

Consequently, while both methods may be affected by inherent experimental errors, the Charpy test is likely to provide an upper bound type of estimate for the fracture energy, when compared with the one-point bend test. Yet, the latter indicates that the fracture energy is significantly greater than that of the Charpy test. This is consistent with the fact that, greater loads and displacements are experienced in one-point bend tests, as shown in Figure 3. Therefore, the greater fracture energy cannot be simply attributed to the fact that different experimental methods are used. Such an observation is consistent with other observations of increasing fracture toughness with the stress-intensity rate which was previously reported, e.g., for polymeric materials (Rittel and Maigre, 1996). In these experiments the initiation toughness increase was shown to correspond to an increased roughness of the fracture surface at initiation (see also Ravi-Chandar and Knauss, 1984). Consequently, additional characterization of the failure mechanisms was carried out, as detailed next. Here it should be added that the Charpy impact energy is usually lower than the energy measured from quasi-static test. This is the case when I12 and I34 specimens are compared. For the tests at lower temperatures (I14 and I37) no conclusion can be drawn because of the scatter inherent to this testing mode.

4.2. On the nature of secondary cracking

The first point to be recalled is that the macroscopic roughness was noted to increase with the loading rate, at least for the specimens tested at about -160 °C. Since the fracture path, including secondary cracking, dictates the roughness, a statistical analysis was carried out on the total number of cracks laying in the wake of the main crack (one side of the specimen only).

Figure 6b shows a Weibull plot of the distribution of microcrack length. This plot is typical of all three specimens and it shows that Weibull distribution represents this distribution satisfactorily, according to:

$$P_R = 1 - \exp\left(-\frac{l}{l_0}\right)^b \tag{2}$$

In this non-dimensional presentation, l is the microcrack length and l0 is a reference length. The parameters of the distribution were determined, including the 95% intervals of confidence limits for each specimen, as summarized in Table 4.

From the statistical analysis, it thus appears, that the crack length distribution can be described using Weibull statistics. Yet, the relatively small sample size (number of specimens and cracks per specimen) does not allow for a further comparison of the various specimens from a statistical point of view.

Another important result is that the total number of microcracks in the specimens tested at low temperature (~ -160 ∘C) is smaller in the quasi-static specimen when compared with

the two other dynamic specimens. This point is consistent with the observed trend in roughness. This observation is to be added to the fact that the apparent number of cleavage origins and their nature did not vary among the various specimens. This indicates that the physical fracture mechanisms, which operate in the lower shelf regime, are the same, regardless of the loading rate. The excess of energy appears to be dissipated by the creation of additional microcracks beneath the main crack. Recent studies devoted to the dynamic fragmentation of brittle ceramics have shown that the number of secondary microcracks and the fracture stress were increasing functions of strain rate (Denoual and Hild, 2000). These observations are in contrast with previous observations of Rittel and Maigre (1996) who could clearly distinguish between the initiation and propagation roughness in polymeric specimens. However, it must be noted that such a clear distinction cannot be easily identified on metallic fracture surfaces as opposed to polymeric. Microcracks in polymeric materials have also been investigated in relation to crack-tip velocity and branching phenomena by Ravi-Chandar and Yang (1997) and by Sharon and Fineberg (1998). These authors investigated rapid crack propagation in brittle polymers, and noted that beyond a certain critical velocity, secondary microcracking developed from the main crack. By contrast, the present microcracks are distributed all along the main crack-path, indicating that the dissipation of excess energy is immediate from the onset of crack propagation. However, it should be kept in mind that the present experiments were carried out with blunt notches as opposed to sharp cracks in the above-mentioned references. It is thus suggested that, whereas the physical fracture mechanisms are identical irrespective of the loading rate, excess fracture energy is dissipated by creating more secondary cleavage microcracks at higher loading rates.

5. Conclusions

Low temperature fracture toughness of 16MND5 (A508) steel was investigated at loading rates ranging from quasi-static to highly transient, through conventional Charpy testing. From the comparison of the various tests, the following conclusions can be made:

- The global energies at the lower shelf are generally observed to increase with the loading rate. This is consistent with increasing levels of loads and displacements to fracture.
- The origin of cleavage initiation can be identified as fracture of inclusions or carbides, in all the cases.
- The number and the nature of operating cleavage origins were not observed to be influenced by the loading rate.
- The macroscopic roughness of the fracture surface increases with the loading rate, at the lowest test temperature.
- Secondary cleavage microcracks are generated beneath the main crack, and they contribute to the observed roughness of the fracture surface.
- At lower temperature, a greater number of microcracks are generated during dynamic testing when compared with quasi-static. This contributes, most likely, to an increased dissipation of fracture energy.
- The statistical distribution of the microcrack length can be satisfactorily described by a Weibull distribution in all the investigated cases.
- Additional work is needed to further establish quantitative statistical estimates related to the influence of the loading rate and temperature in the microcrack distribution.

Acknowledgement

Dr L. Rota (CTA) and Mr J. Clisson (CTA) are acknowledged for their assistance. Y. Grandjean (Electricité de France) is also acknowledged.

References

Aoki, S. and Kimura, T. (1993). Finite element study of the optical method of caustic for measuring impact fracture toughness. *Journal of Mechanics and Physics of Solids* **41**(3), 413–425.

Böhme, W., Kalthoff, JF. (1982). The behavior of notched bend specimens in impact testing. *International Journal of Fracture* **20**, R139–R143.

Böhme, W. (1990). Dynamic key-curves for brittle fracture impact tests and establishment of a transition time. ASTM STP 1074, Judas, G.P. et al. (eds.), pp. 144–156.

Charpy, M.G. (1901). Note sur l'essai des métaux Charpy, M.G., (1901), Note sur l'essai des métaux à la flexion par choc de barreaux entaillés. *Mémoires et Compte-rendus de la Société des Ingénieurs Civils de France*, June 1901, 848–877.

Denoual, C. and Hild, F. (2000). A damage model for the dynamic fragmentation of brittle solids. *Computer methods in applied mechanics and engineering* **183**, 247–258.

Lautridou, J.C. and Pineau, A. (1981). Crack initiation and stable crack growth resistance in A508 steels in relation to inclusion distribution. *Engineering Fracture Mechanics.* **15**(1–2), 55–71.

Maigre, H. and Rittel D. (1996). Dynamic fracture detection using the force-displacement reciprocity: application to the compact compression specimen. *International Journal of Fracture* **73**(1), 67–79.

Radakovic, Z., Lenkey, G.B., Grabulov, V. and Sedmak, A. (1999). Application of two independent measurement techniques for determination of ductile crack growth initiation. *International Journal of Fracture* **96**, L23–L28.

Ravi-Chandar, K. and Knauss, W.G. (1984). An experimental investigation into dynamic fracture: II. Microstructural aspects. *International Journal of Fracture* **26**, 65–80.

Ravi Chandar, K. and Yang, B. (1997). On the role of microcracks in the dynamic fracture of brittle materials. *Journal of Mechanics and Physics of Solids* **45**(4), 535–563.

Rittel, D. (1998). The influence of temperature on dynamic failure mode transitions. *Mechanics of Materials* **30**(3), 217–227.

Rittel, D. and Maigre, H. (1996). An investigation of dynamic crack initiation in PMMA. *Mechanics of Materials* **28**, 229–239.

Rittel, D., Pineau, A., Clisson, J. and Rota, L. (2002). On testing of Charpy specimens using the one point bend impact technique. *Experimental Mechanics* (in press).

Rosakis, A.J. and Ravichandran, G. (2000). Dynamic failure mechanics. *International Journal of Solids and Structures* **37**, 331–348.

Ruiz, C. and Mines, R.A.W. (1985). The Hopkinson pressure bar: an alternative to the instrumented pendulum for Charpy tests. *International Journal of Fracture* **29**, 101–109.

Server, W. (1985). Charpy Impact Testing. *In* ASM Metals Handbook, Vol. 8, ASM, Metals Park, OH.

Sharon, E. and Fineberg, J. (1998). Universal features of the microbranching instability in dynamic fracture. *Philosophical Magazine B* **78**(2), 243–251.

Tanguy, B. Piques, R., Laiarinandrasana, L. and Pineau, A. (2000). Notch stress strain distribution in Charpy V specimen /experiments and modeling. Proceedings ECF 13, Fracture Mechanics: Applications and Challenges. Elsevier Science.